Lateral Proton Diffusion Rates along Stearic Acid Monolayers

Christopher J. Slevin and Patrick R. Unwin*

Contribution from the Department of Chemistry, University of Warwick, Coventry CV4 7AL, U.K.

Received August 31, 1999

Abstract: Proton in-plane lateral diffusion rates in Langmuir monolayers have been measured as a function of surface coverage, with a sensitivity not possible previously, using scanning electrochemical microscopy (SECM) operating in the induced desorption mode. With this approach an acidic monolayer, spread at the air/water interface, is deprotonated locally, by reducing protons in solution to hydrogen at an ultramicroelectrode probe, which drives the acid dissociation reaction. In turn, this creates a proton diffusion gradient in the solution and at the interface, and the transport-limited current flowing at the electrode provides a measure of the rates of diffusion in these two environments. Measurements on stearic acid monolayers at the air/water interface clearly show that in-plane lateral proton diffusion occurs, but the diffusion coefficient depends critically on the physical state of the monolayer, and is at most only ca. 15% of the magnitude in bulk solution.

Introduction

A key step in bioenergetic processes in cell membranes is the movement of protons between source and sink sites.[1] Lateral diffusion along the cell membrane is a potentially efficient pathway for proton transfer[2−4] compared with the alternative mode of transport, involving desorption and diffusion through solution. However, the degree to which the surface diffusion pathway operates is a matter of some controversy, due to contradictory results obtained by different experimental techniques.[2,5−9]

A popular method measures the dispersion of protons under a Langmuir monolayer by measuring fluorescence intensity changes of pH-sensitive fluorescent probe molecules, within the monolayer, at an observation point several centimeters away from a mechanically stirred compartment into which an acid solution is initially injected.[6] These studies suggest that protons are transported along lipid/aqueous[6] and even protein/aqueous[6i] interfaces predominantly by lateral diffusion. In initial studies, the lateral proton diffusion coefficient was considered to be at least 20 times that in aqueous solution,[6d] although in later work it was simply reported that lateral diffusion was facilitated. These results have been disputed, with arguments that convection may contribute to the high rates observed,[5a] although similar conclusions were reached from *dc* conductance measurements.[8,9] In contrast, laser pulse studies in vesicles[5] found no evidence for unusually high lateral proton mobility. In fact, the observation of adsorption/desorption on a rapid (microsecond) time scale suggested that the in-plane mobility would be retarded severalfold compared to bulk aqueous solution.[5,10]

In this paper we report new scanning electrochemical microscopy (SECM) studies for investigating lateral proton diffusion in Langmuir monolayers at an air/water interface. We focus on stearic acid as an initial model system, since lateral diffusion, via a hop and turn mechanism,[6e] involving water molecules close to the interface, has been suggested to explain the enhanced conductance observed on compression of stearic acid monolayers.[8b,11] The SECM[12] was operated in the induced desorption (SECMID) mode,[13] which is one of a family of equilibrium perturbation-based approaches.[14] This approach was recently applied in a Langmuir trough to study the effects of 1-octadecanol on oxygen transfer rates across an air/water interface.[14e] The application of SECM in this environment could be viewed as generally building on the use of microelectrochemistry to study lateral diffusion in films of amphiphiles assembled at the air/water interface.[15]

* Author to whom correspondence should be sent.

(1) Gennis, R. B. *Biomembranes: Molecular Structure and Function*; Springer-Verlag: New York, NY, 1989.

(2) Scherrer, P. *Nature* **1995**, *374*, 222.

(3) Kell, D. B. *Biochim. Biophys. Acta* **1979**, *549*, 55.

(4) Westerhoff, H. V.; Melandri, B. A.; Venturolli, G.; Azzone, G. F.; Kell. D. B. *FEBS Lett.* **1984**, 165.

(5) (a) Gutman, M.; Nachliel, E. *Biochim. Biophys. Acta* **1995**, *1231*, 123. (b) Nachliel, E.; Gutman, M. *J. Am. Chem. Soc.* **1988**, *110*, 2629. (c) Yam, R.; Nachliel, E.; Gutman, M. *J. Am. Chem. Soc.* **1988**, *110*, 2636. (d) Kasianowicz, J.; Benz, R.; Gutman, M.; McLaughlin, S. *J. Membr. Biol.* **1987**, *99*, 225.

(6) (a) Gabriel, B.; Teissié, J. *J. Am. Chem. Soc.* **1991**, *113*, 8818. (b) Prats, M.; Gabriel, B.; Teissié, J. *J. Am. Chem. Soc.* **1993**, *115*, 10153. (c) Prats, M.; Tocanne, F.; Teissié, J. *Eur. J. Biochem.* **1987**, *162*, 379. (d) Teissié, J.; Prats, M.; Soucaille, P.; Tocanne, F. *Proc. Natl. Acad. Sci. U.S.A.* **1985**, *82*, 3217. (e) Prats, M.; Tocanne, F.; Teissié, J. *Eur. J. Biochem.* **1985**, *149*, 663. (f) Prats, M.; Tocanne, F.; Teissié, J. *J. Membr. Biol.* **1987**, *99*, 225. (g) Tocanne, F.; Teissié, J. *Biochim. Biophys. Acta* **1990**, *1013*, 111. (h) Gabriel, B.; Prats, M.; Teissié, J. *Biochim. Biophys. Acta* **1994**, *1186*, 172. (i) Gabriel, B.; Teissié, J. *Proc. Natl. Acad. Sci. U.S.A.* **1996**, *93*, 14521.

(7) Scherrer, P. *Nature* **1996**, *379*, 306.

(8) (a) Morgan, H.; Taylor, D. M.; Oliveira, O. N., Jr. *Chem. Phys. Lett.* **1980**, *150*, 311. (b) Morgan, H.; Taylor, D. M.; Oliveira, O. N., Jr. *Biochim. Biophys. Acta* **1991**, *1062*, 149.

(9) (a) Sakurai, I.; Kawamura, Y. *Biochim. Biophys. Acta* **1987**, *904*, 405. (b) Sakurai, I.; Kawamura, Y. *Biochim. Biophys. Acta* **1989**, *985*, 347.

(10) Deamer, D. W.; Nichols, J. W. *J. Membr. Biol.* **1989**, *107*, 91.

(11) (a) Cavalli, A.; Oliveira, O. N., Jr. *Rev. Sci. Instrum.* **1995**, *66*, 5567. (b) Leite, V. B. P.; Cavalli, A.; Oliveira, O. N., Jr. *Phys. Rev. E* **1998**, *57*, 6835.

(12) For reviews of SECM see for example: (a) Bard, A. J.; Fan, F.-R. F.; Pierce, D. T.; Unwin, P. R.; Wipf, D. O. *Science* **1991**, *254*, 68. (b) Bard, A. J.; Mirkin, M. V.; Fan, F.-R. F. *Electroanal. Chem.* **1993**, *18*, 243. (c) Mirkin, M. V. *Anal. Chem.* **1996**, *68*, 177A. (d) Barker, A. L.; Gonsalves, M.; Macpherson, J. V.; Slevin, C. J.; Unwin, P. R. *Anal. Chim. Acta* **1999**, *385*, 223.

(13) Unwin, P. R.; Bard, A. J. *J. Phys. Chem.* **1992**, *96*, 5035.

(14) (a) Macpherson, J. V.; Unwin, P. R. *J. Phys. Chem.* **1994**, *98*, 1704. (b) Macpherson, J. V.; Hillier, A. C.; Unwin, P. R.; Bard, A. J. *J. Am. Chem. Soc.* **1996**, *118*, 6445. (c) Slevin, C. J.; Umbers, J. A.; Atherton, J. H.; Unwin, P. R. *J. Chem. Soc., Faraday Trans.* **1996**, *92*, 5177. (d) Barker, A. L.; Macpherson, J. V.; Slevin, C. J.; Unwin, P. R. *J. Phys. Chem. B* **1998**, *102*, 1586. (e) Slevin, C. J.; Ryley, S.; Walton, D. J.; Unwin, P. R. *Langmuir* **1998**, *14*, 5331.

10.1021/ja993148v CCC: $19.00
Published on Web 03/04/2000

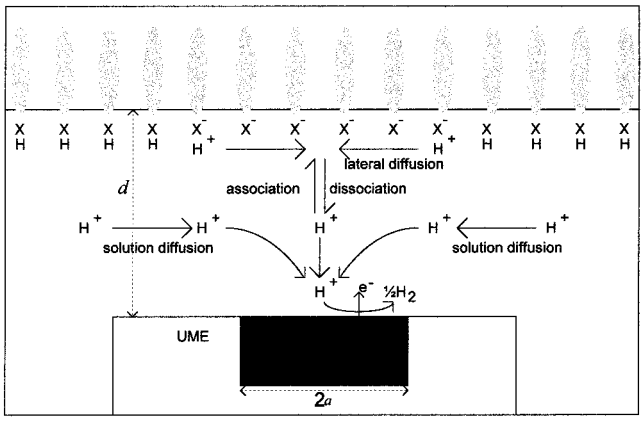

Figure 1. Schematic (not to scale) of the arrangement for SECM measurements of proton transport at a stearic acid monolayer deposited at the air/water interface. The UME typically had a diameter, 2*a*, in the range 10−25 μm and the tip/interface distance, *d*, was typically $\leq 2a$.

Principles

The principles of the SECMID approach[13,14] will be outlined briefly here as they apply to the system of interest. SECMID uses a disk-shaped ultramicroelectrode (UME, 10−25 μm in diameter) positioned in the aqueous phase in a Langmuir trough, at a small distance, *d*, below the air/stearic acid/water interface (see Figure 1). This distance is typically of the order of the electrode radius, *a*, or smaller. The association/dissociation reaction at the interface, involving the surface-bound amphiphile,

$$C_{17}H_{35}COOH_{surface} \rightleftarrows C_{17}H_{35}COO^-{}_{surface} + H^+{}_{aq} \quad (1)$$

is initially at equilibrium, controlled by the concentration of acid in the aqueous phase. A potential is then applied to the UME, such that $H^+{}_{aq}$ is reduced to H_2 at a diffusion-controlled rate at the electrode, thus depleting the concentration of protons in the thin gap between the electrode and the air/water interface. This serves to drive the diffusion of protons through solution into the depleted region, as well as perturbing the established equilibrium (eq 1), by promoting the deprotonation of the stearic acid molecules (Figure 1). The deprotonation of surface-confined stearic acid occurs in a spot of similar dimensions to the UME, generating a radial surface proton concentration gradient that provides the driving force for lateral proton diffusion. In principle, $C_{17}H_{35}COOH$ and $C_{17}H_{35}COO^-$ may diffuse along the surface, in to and out of the depleted region, but the diffusion rates for these macromolecular amphiphiles are expected to be considerably lower[15] than the H^+ diffusion rate, and we may neglect this process.

The current response is governed by the flux of protons at the electrode surface, which is in turn controlled by the three modes of proton transport: protonation/deprotonation, solution diffusion, and surface diffusion (Figure 1).[13] Under the well-defined and calculable mass-transport conditions of SECM, these three processes may be resolved over the full range of surface pressures. In particular, the ability to combine transient measurements, at a fixed UME−interface distance, where protonation/deprotonation dominates, with steady-state measurements, made over a range of UME separations, where surface diffusion influences the proton flux more strongly, enables both the lateral diffusion coefficient and the protonation/deprotonation rates to be determined.[13]

Theory

Analysis of the experimentally measured current data used an earlier model derived for proton adsorption/desorption at a TiO_2 single-crystal surface,[13] with some modifications.

In the presence of excess supporting electrolyte, mass transport of H^+ to the UME is by diffusion in the axisymmetric cylindrical geometry of the SECM,

$$\frac{\partial c}{\partial t} = D_{sol}\left[\frac{\partial^2 c}{\partial r^2} + \frac{1}{r}\frac{\partial c}{\partial r} + \frac{\partial^2 c}{\partial z^2}\right] \quad (2)$$

where c and D_{sol} are the concentration and diffusion coefficient of H^+ in solution, r and z are the coordinates in the radial and normal directions relative to the electrode surface starting at its center, and t is time. Initially, the concentration of H^+ in the solution is equal to the bulk concentration, c^*,

$$t = 0, \text{ all } r, 0 < z < d: \qquad c = c^* \quad (3)$$

The concentration distribution of H^+ at the probe electrode surface following the potential step is governed by,

$$z = 0, 0 \leq r \leq a: \qquad c = 0 \quad (4)$$

$$z = 0, a < r \leq r_s: \qquad D_{sol}(\partial c/\partial z) = 0 \quad (5)$$

where r_s is the radial distance from the center of the electrode to the edge of the insulating glass sheath surrounding the electrode. In typical experimental practice, $r_s \geq 10a$. Further boundary equations define a condition of zero radial flux at the center of symmetry, $r = 0$, and the recovery of the initial proton concentration beyond the radial edge of the tip−substrate domain,[16]

$$r = 0, 0 < z < d: \qquad D_{sol}(\partial c/\partial r) = 0 \quad (6)$$

$$r > r_s, 0 < z < d: \qquad c = c^* \quad (7)$$

The substrate surface boundary condition depends on the deprotonation/protonation process, surface diffusion, and the surface site density. The acid dissociation constant for eq 1,

$$K_a = [RCOO^-][H^+]/[RCOOH] \quad (8)$$

will depend on the degree of surface ionization,[13,17] and may be written in terms of a potential-independent (intrinsic) dissociation constant, K_a^i,

$$K_a = K_a^i \exp(F\psi_0/RT) \quad (9)$$

where ψ_0 is the surface potential, F is Faraday's constant, and R and T have their usual meanings. The surface potential−charge density relationship can be calculated using the Gouy−Chapman model,[13] which, for a symmetrical electrolyte, is given by

$$\sigma_0 = (8\epsilon\epsilon_0 RTI)^{1/2} \sinh(F\psi_0/2RT) \quad (10)$$

where σ_0 is the charge density, ϵ is the dielectric constant, ϵ_0 is the permittivity of free space, and I is the ionic strength of the

(15) (a) Kim, J. S.; Lee, S. B.; Kang, Y. S.; Park, S. M.; Majda, M.; Park, J. *J. Phys. Chem. B* **1998**, *102*, 5794. (b) Charych, D. H.; Goss, C. A.; Majda, M. *J. Electroanal. Chem.* **1992**, *323*, 339. (c) Charych, D. H.; Landau, E. M.; Majda, M. *J. Am. Chem. Soc.* **1991**, *113*, 3340.

(16) Kwak, J.; Bard, A. J. *Anal. Chem.* **1989**, *61*, 1221.

(17) (a) Sun, L.; Crooks, R. M.; Ricco, A. J. *Langmuir* **1993**, *9*, 1775. (b) White, H. S.; Peterson, J. D.; Cui, Q.; Stevenson, K. J. *J. Phys. Chem. B* **1998**, *102*, 2930 and references therein.

solution. The developing negative charge that occurs under SECMID deprotonation defines the surface charge density,

$$\sigma_0 = F(\theta - 1)N \tag{11}$$

where θ is the fraction of undissociated stearic acid molecules, and N is the total surface density of stearic acid/stearate.

The rate constants defining the kinetics of association/dissociation at the interface, k_a (cm s^{-1}) and k_d (mol cm^{-2} s^{-1}), respectively, may also be expressed in terms of potential-independent (intrinsic) rate constants, k_a^i and k_d^i,

$$k_a = k_a^i \exp(-F\psi_0/2RT) \tag{12}$$

$$k_d = k_d^i \exp(F\psi_0/2RT) \tag{13}$$

The Gouy−Chapman approach to calculating the surface potential−charge density relationship has been shown to be valid for ionic strengths up to the order employed in the studies herein, and for areas per charge down to 40−50 $Å^2$,[18] which covers the range of the current experiments. The initial surface charge density and potential are calculated when the deprotonation/protonation process is at equilibrium. θ depends on the equilibrium constant according to the following expression,

$$z = d,\ 0 < r < r_s: \qquad \theta = c/(K_a + c) \tag{14}$$

An initial guess of θ can be obtained using the value of K_a^i in eq 14. Equations 9, 10, 11, and 14 can then be solved in an iterative fashion to establish the true initial state.

By dissociating the monolayer with a UME, the local surface density changes due to the accumulation of negative charge, and this might alter the local structure of the monolayer. However, such effects are only expected to be significant when there are major perturbations in the degree of surface ionization,[18] and we will show later that the induced changes in θ, under SECMID conditions, are relatively small.

Surface diffusion, coupled with acid association/dissociation, defines the boundary condition at the target interface,

$$z = d,\ 0 \le r \le r_s: \qquad N(\partial\theta/\partial t) = ND_{sur}[\partial^2\theta/\partial r^2 + (1/r)(\partial\theta/\partial r)] - k_d\theta + k_a c(1 - \theta) \tag{15}$$

for which additional constraints apply,

$$z = d,\ r = 0: \qquad \partial\theta/\partial r = 0 \tag{16}$$

$$z = d,\ r > r_s: \qquad \theta = c^*/(K_a + c^*) \tag{17}$$

In eq 15, D_{sur} is the surface diffusion coefficient. In treating lateral diffusion using eq 15, we are considering that for a given surface density of amphiphiles, the surface diffusion coefficient is uniform over the region of interest. This is likely to be a good assumption since, as discussed below, the degree of surface ionization does not change appreciably under SECMID conditions on the present system. Moreover, eq 15 assumes that lateral diffusion is due to surface bound protons.

The problem was solved using the alternating direction implicit (ADI) finite difference method,[19] and the SECM current response was simulated as described previously.[13,19]

Experimental Section

Solutions. Aqueous solutions were prepared using Milli-Q-reagent water (Millipore Corp., resistivity ≥ 18 MΩ cm). Solutions contained 2×10^{-5} to 5×10^{-4} mol dm^{-3} HNO_3 (Sigma-Aldrich, Gillingham, U.K.) and 0.1 mol dm^{-3} KNO_3 (A.R., Fisher, Loughborough, U.K.) as supporting electrolyte. Ferrocyanide solutions contained 1×10^{-3} mol dm^{-3} potassium hexacyanoferrate (A.R., Fisher) and 0.1 mol dm^{-3} potassium chloride (BDH AnalaR, Merck, Lutterworth, U.K.). Stearic acid (99+%, Sigma-Aldrich) solutions used to prepare the monolayer typically contained 1 mg of stearic acid/mL of solvent (chloroform, A.C.S., Sigma-Aldrich).

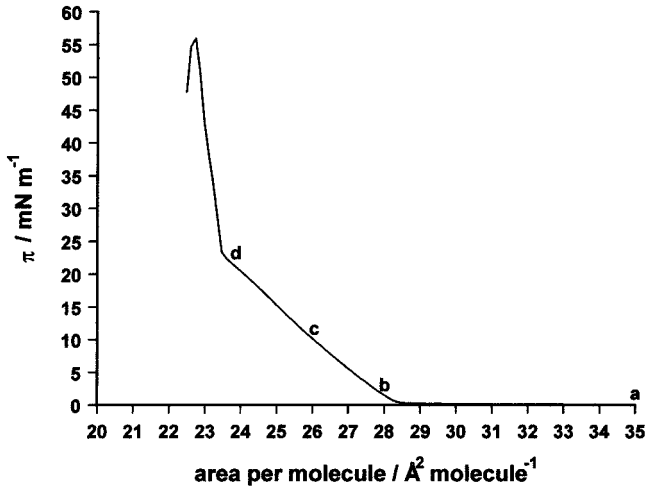

Figure 2. Pressure (π)−area (A) isotherm for stearic acid on an aqueous subphase containing 0.1 mol dm^{-3} KNO_3 and 5×10^{-5} mol dm^{-3} HNO_3. The labels a−d correspond to the data in Figure 5.

Apparatus. The Langmuir trough (model 611, Nima Technology, Coventry, U.K.) was housed inside a glovebox (Glovebox Technology, Huntingdon, U.K.) purged with Argon (Pureshield, BOC Gases, Guildford, U.K.). Monolayers were observed using Brewster angle microscopy (MiniBAM Brewster Angle Microscope, Nanofilm Technologie GmbH, Göttingen, Germany). The electrode was positioned using a set of x,y,z stages (M-462, Newport Corp., CA) and a piezoelectric positioner and controller (models P-843.30 and E662, Physik Instrumente, Germany). The procedure for the fabrication of submarine UMEs has been described previously.[14c] The platinum UMEs used were 25 or 10 μm in diameter.

Procedures. Monolayers of stearic acid were formed by depositing a known volume (typically 50 ± 1 μL) of the stearic acid solution on the subphase, dropwise, using a microliter syringe (100 μL volume, Hamilton, Reno, NV). The solvent was allowed to evaporate for 15 min before measurements were made. Pressure−area isotherms were recorded at a surface area compression rate of 25 cm^2 min^{-1}, from a surface area of 500 cm^2. The solvent itself caused no discernible rise in surface pressure when spread without surfactant.

Electrochemical measurements employed a two-electrode arrangement, with a Pt submarine working electrode, and a silver quasireference electrode (AgQRE). Current−time transients were recorded using a digital storage oscilloscope (NIC310, Nicolet, Coventry, U.K.) at a fixed UME−interface distance. A reproducible response was achieved by pretreating the electrode each time by first oxidizing at 1.3 V vs AgQRE for 3 s, then stepping the potential to −0.59 V for 1 min to condition the electrode, before stepping to −0.8 V to effect the diffusion-controlled reduction of H^+. Current−distance tip approach curves were recorded in a similar way to previous studies.[14e] The electrode, initially at a distance ca. 30 μm from the air/water interface, was anodically pretreated as described above, before the potential was stepped to −0.8 V for the steady-state reduction of H^+. After a stable current had been attained for ca. 1 min, the electrode was scanned toward the air/water interface, at a velocity of 0.6 μm s^{-1}, while the current and distance were recorded simultaneously. Each time the interfacial area was changed, a few minutes were allowed for the monolayer to stabilize.

Results and Discussion

The pressure (π)−area (A) isotherm for stearic acid on an aqueous subphase containing 0.1 mol dm^{-3} KNO_3 and 5×10^{-5} mol dm^{-3} HNO_3 is given in Figure 2. On compression, the

(18) Spink, J. A. *J. Colloid Sci.* **1963**, *18*, 512.
(19) Unwin, P. R.; Bard, A. J. *J. Phys. Chem.* **1991**, *95*, 7814.

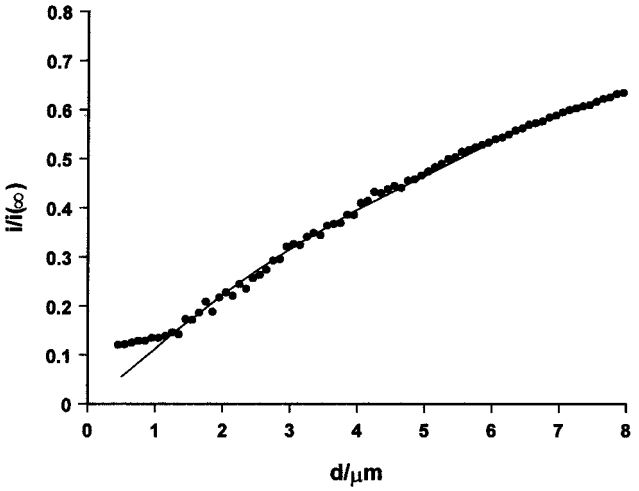

Figure 3. Normalized steady-state diffusion-limited current vs UME−interface separation for the oxidation of 1×10^{-3} mol dm^{-3} ferrocyanide at a 10 μm diameter platinum UME approaching an air/water interface with a stearic acid monolayer at a surface coverage of 26 Å^2 molecule^{-1} (●). The solid line is the theoretical curve for hindered solution diffusion.

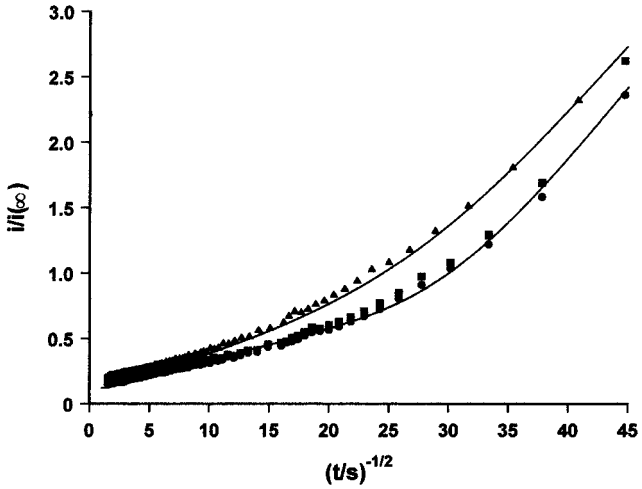

Figure 4. Current−time data for the reduction of H^+ (5×10^{-4} mol dm^{-3} HNO_3) at a 25 μm diameter UME positioned close ($d/a = 0.2$) to the air/water interface for (●) a clean surface and with a stearic acid monolayer at (■) 38 and (▲) 26 Å^2 molecule^{-1}. The lower solid line is the theoretical response for hindered solution diffusion only, while the upper line corresponds to diffusion-controlled deprotonation/protonation of the interface ($pK_a^i = 4.7$) and a surface coverage of 26 Å^2 molecule^{-1}.

isotherm exhibits the expected liquid-condensed (L_2) and superliquid (LS) phases,[20] for molecular areas between 28.5 and 23.5 Å^2 molecule^{-1} and 23.5−22.7 Å^2 molecule^{-1}, respectively. At larger surface areas per molecule, before a detectable rise in the surface pressure was observed, Brewster angle microscopy (BAM) of the monolayer indicated that there were two coexisting phases, namely the L_2 and G (gaseous) phases.

It was previously demonstrated[14e] that the presence of a probe UME in close proximity to a monolayer of 1-octadecanol spread at the air/water interface caused no apparent physical disruption to the monolayer. Recent studies of monolayers at liquid/liquid interfaces also support the validity of using SECM to investigate monolayer systems noninvasively.[21,22] Confirmation that this was also the case for stearic acid, and particularly that the monolayer did not affect the electrode response, was sought through measurements of the electrode response for the oxidation of ferrocyanide close to a stearic acid monolayer. Typical data are given in Figure 3, in the form of a plot of the current, i, normalized with respect to the steady-state current with the tip at an effectively infinite distance from the interface, $i(\infty)$, as a function of tip−interface distance, d. The results shown are for a surface coverage of 26 Å^2 molecule^{-1}, corresponding to a pressure of 10.0 mN m^{-1}, but an identical response was obtained at all surface pressures from 0 mN m^{-1} up to around 50 mN m^{-1}. The current−distance response displayed only hindered diffusion characteristics, conforming to the predicted negative feedback behavior.[16] The distance of closest approach of the electrode to the monolayer, which is used subsequently as a fitting parameter, is determined from these, and other control, experiments.

Potential step transients were used to probe the association/dissociation process, with negligible influence from lateral surface diffusion, by employing a relatively high concentration of protons (5.0×10^{-4} mol dm^{-3} HNO_3) in the aqueous solution. The localized depletion of H^+ in the electrode−interface gap drives the deprotonation reaction, releasing H^+ from the surface-confined amphiphile. The resulting current−time response depends on the rates of the protonation and deprotonation processes. Typical data obtained from these experiments are displayed in Figure 4 in the form of normalized current vs $t^{-1/2}$ plots, to emphasize the short time behavior, where deprotonation dominates.[13] These data were obtained with a 25 μm diameter Pt electrode at an electrode−surface separation, d/a, of 0.2, and were made at a range of surface pressures. The data are plotted alongside simulated results for the protonation/deprotonation process, using a pK_a^i of 4.7 and intrinsic rate constants of 16 cm s^{-1} and 3.2×10^{-7} mol cm^{-2} s^{-1}, respectively. The pK_a^i value is consistent with previously reported pK_a^i values between 4.7[23] and 4.9.[18] The rate constant values indicate diffusion control of the overall process; larger rate constants in the model resulted in the same response.

Over the range of surface pressures of interest (>0.1 mN m^{-1}), potential step chronoamperometric data were consistent with a diffusion-controlled protonation/deprotonation process on the SECM time scale, as expected with $pK_a^i = 4.7$.[5] For the conditions of interest in this study, the pK_a^i value is expected to be relatively insensitive to surface pressure.[18] Surface diffusion is not important in these theoretical fits, since the interfacial diffusion rates are too low to contribute to the current response of the electrode, due to the relatively high solution concentration of protons, which dominates the current signal. SECM-driven deprotonation was undetectable at large surface areas (surface pressures below 0.1 mN m^{-1}) as shown in Figure 4. Based on the Brewster angle microscopy studies, under these conditions, there is a high probability that the UME just sees a pure water/air interface.

Lateral proton diffusion effects were investigated via steady-state approach curves, in which the current was measured as a function of d, at lower solution H^+ concentrations (2×10^{-5} to 5×10^{-5} mol dm^{-3} HNO_3). The lowest experimental approach curve in Figure 5 is the response recorded with a clean air/water interface. From this curve it is seen that as the electrode approaches the interface, the current decreases due to a

(20) Bibo, A. M.; Peterson, I. R. *Adv. Mater.* **1990**, *2*, 309.
(21) Tsionsky, M.; Bard, A. J.; Mirkin, M. V. *J. Am. Chem. Soc.* **1997**, *119*, 10785.
(22) Delville, M. H.; Tsionsky, M.; Bard, A. J. *Langmuir* **1998**, *14*, 2774.
(23) Martin, P.; Szablewski, M. *Nima Technology, Tensiometers and Langmuir−Blodgett Troughs, Operating Manual*, 4th ed.; Grunfeld, F., Ed.; Nima Technology Ltd.: 1998.

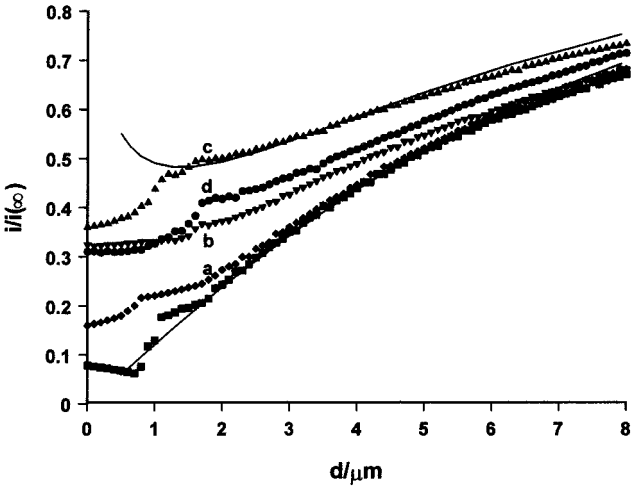

Figure 5. Normalized steady-state diffusion-limited current vs UME−interface separation for the reduction of 5×10^{-5} mol dm^{-3} H^+ at a 10 μm diameter platinum UME approaching an air/water interface, for (■) a clean surface and with a stearic acid monolayer at a surface coverage of (◆) 35 (a), (▼) 28 (b), (▲) 26 (c), and (●) 24 Å^2 molecule^{-1} (d). The lower solid line is the theoretical curve for hindered solution diffusion only, while the upper solid line is for a stearic acid covered interface (26 Å^2 molecule^{-1}) with a surface diffusion coefficient of 1.2×10^{-5} cm^2 s^{-1}. The labels a−d correspond to the surface pressures shown in Figure 2.

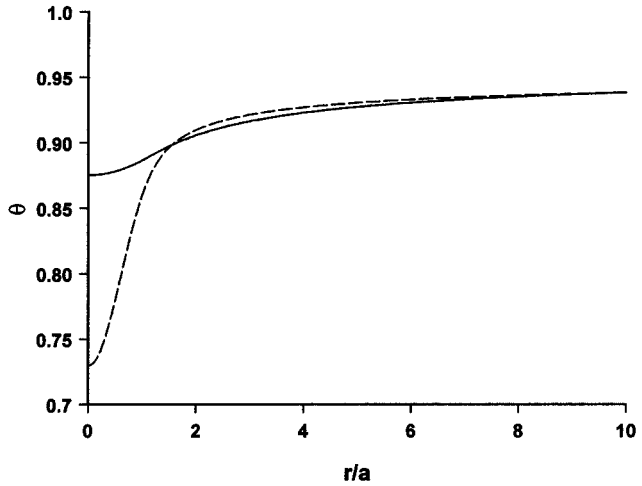

Figure 6. Calculated steady-state radial distribution of θ across a monolayer. The position, $r = 0$, coincides with the cylindrical axis of the probe UME. The simulation used $a = 5$ μm, $d = 2$ μm, $N = 6.4 \times 10^{-10}$ mol cm^{-2}, and $c^* = 5 \times 10^{-5}$ mol dm^{-3}. The solid curve corresponds to a surface diffusion coefficient, D_{sur}, of 1.2×10^{-5} cm^2 s^{-1}, while the dashed curve was calculated without surface diffusion present.

diminishing flux of protons at the electrode, as a consequence of hindered diffusion. When the electrode reaches a distance of approximately 1.5 μm from the interface, the experimental approach curve begins to deviate from the theoretical curve, probably because the interface distorts to accommodate the electrode, particularly the glass insulating sheath surrounding the electrode. This effect is observed in all of the approach curves, and is used to assign a distance of closest approach of the electrode to the interface.[24] The data are only analyzed at $d > 1.5$ μm, where these effects are unimportant. Theoretically generated current−distance approach curves were fitted to the data to allow the contribution of lateral proton diffusion to be determined. Much of the data in Figure 5, obtained at $c^* = 5 \times 10^{-5}$ mol dm^{-3}, at a range of surface compressions, show current enhancements above the level for an inert interface. The current enhancements, which depend on the surface area of the monolayer, may be attributed to in-plane lateral proton diffusion at the air/water interface, contributing an increased flux of H^+ to the 10 μm diameter UME used for these studies.

The lateral proton diffusion coefficient may be evaluated since other variables (surface coverage, protonation/deprotonation kinetics, pK_a, solution diffusion coefficient, electrode size, electrode-interface separation, H^+ concentration, and ionic strength) are all known. The surface diffusion rate depends critically on the degree of compression of the monolayer, starting at an undetectable level at surface pressures below 0.1 mN m^{-1}, where the system is in an L_2/G phase coexistence, and increasing when the monolayer is compressed sufficiently to enter the L_2 phase. The maximum surface diffusion coefficient of $1.2(\pm 0.1) \times 10^{-5}$ cm^2 s^{-1} occurred at a pressure of 9−10 mN m^{-1}, corresponding to a surface coverage of ca. 26 Å^2 molecule^{-1}. This compares with a proton diffusion coefficient in bulk solution of 8.0×10^{-5} cm^2 s^{-1}. Further compression of the monolayer, below 26 Å^2 molecule^{-1}, in discrete intervals in surface pressure of ca. 5 mN m^{-1}, up to ca. 35 mN m^{-1} in the LS state, caused the surface diffusion rate to fall, an observation consistent with the prediction of an optimum intermolecular separation for the formation of an H-bonded network across the monolayer surface.[11] Results obtained with electrodes of diameter 10−25 μm, and with HNO_3 concentrations of 2×10^{-5} and 5×10^{-5} mol dm^{-3}, were fairly consistent with those presented in Figure 5. The maximum surface diffusion coefficient always occurred at the same surface pressure, and had a value of $6(\pm 1) \times 10^{-6}$ cm^2 s^{-1}, when measured with a 25 μm diameter electrode, at an HNO_3 concentration of 2×10^{-5} mol dm^{-3}.

The processes occurring at the air/water interface during SECMID may be understood by analyzing the distribution of the predicted fraction of protonated molecules, θ, across the surface. Figure 6 displays a theoretically simulated θ vs normalized radial distance, r/a, profile. The conditions used in the simulation were similar to those used to obtain the data in Figure 5, with surface coverage $N = 6.4 \times 10^{-10}$ mol cm^{-2} and $d = 2$ μm and with D_{sur} set at 1.2×10^{-5} cm^2 s^{-1} and zero. By comparing the two profiles in Figure 6, the effect of the surface diffusion process can be seen to feed protons along the surface into the depleted region. This extra source of protons is subsequently detected at the electrode, and is responsible for enhancing the current flow. This plot is also important in demonstrating that the fraction of ionized molecules does not change appreciably during a measurement. The degree of ionization changes from a value of ca. 6%, under initial equilibrium conditions, to at most, 12%, in the region of the interface directly above the electrode ($r/a = 0$) as the SECMID response tends toward steady state. The latter value corresponds to a low overall charge density of the order of 200 Å^2/charged molecule, and a small local perturbation of the charge density, which was assumed in the derivation of the theoretical model.

Conclusions

SECMID has been shown to be a powerful technique for quantitatively probing lateral proton diffusion at molecular monolayers, under well-defined conditions. For stearic acid

(24) Barker, A. L.; Unwin, P. R.; Amemiya, S.; Zhou, J.; Bard, A. J. *J. Phys. Chem. B* **1999**, *103*, 7260.

monolayers, under conditions where the majority of molecules are protonated, the degree of lateral diffusion depends critically on the state of the monolayer, but the lateral diffusion coefficient is never more than 15% of the bulk solution value. The lateral proton diffusion coefficients measured in this study contradict the suggestions that surface diffusion in this system should be faster than in bulk solution.[11] Experiments will now be carried out to determine the rate of proton transfer along phospholipid and mixed phospholipid/protein monolayers, to resolve the long-standing controversy regarding the movement of protons between source and sink sites in biomembranes.

Acknowledgment. We thank the BBSRC (88/B10498) for support of this work.

JA993148V